Structural Basis of RasGRP Binding to High-Affinity PKC Ligands

Suo-Bao Rong,[†] Istvan J. Enyedy,[†] Lixin Qiao,[†,‡] Lianyun Zhao,[†] Dawei Ma,[§] Larry L. Pearce,[∥] Patricia S. Lorenzo,[∥] James C. Stone,[⊥] Peter M. Blumberg,[∥] Shaomeng Wang,*[,†] and Alan P. Kozikowski*[,†]

Drug Discovery Program, Department of Neurology, Georgetown University Medical Center, 3970 Reservoir Road, Washington, D.C. 20007, Molecular Mechanisms of Tumor Promotion Section, National Cancer Institute, Bethesda, Maryland 20892, 123, State Key Laboratory of Bio-organic and Natural Chemistry, Shanghai Institute of Organic Chemistry, Chinese Academy of Sciences, 354 Fenglin Lu, Shanghai 200032, China, and Department of Biochemistry, University of Alberta, Edmonton, Alberta T6G 2H7, Canada

Received September 7, 2001

The Ras guanyl releasing protein RasGRP belongs to the CDC25 class of guanyl nucleotide exchange factors that regulate Ras-related GTPases. These GTPases serve as switches for the propagation and divergence of signaling pathways. One interesting feature of RasGRP is the presence of a C-terminal C1 domain, which has high homology to the PKC C1 domain and binds to diacylglycerol (DAG) and phorbol esters. RasGRP thus represents a novel, non-kinase phorbol ester receptor. In this paper, we investigate the binding of indolactam(V) (ILV), 7-(*n*-octyl)-ILV, 8-(1-decynyl)benzolactam(V) (benzolactam), and 7-methoxy-8-(1-decynyl)benzolactam(V) (methoxylated benzolactam) to RasGRP through both experimental binding assays and molecular modeling studies. The binding affinities of these lactams to RasGRP are within the nanomolar range. Homology modeling was used to model the structure of the RasGRP C1 domain (C1-RasGRP), which was subsequently used to model the structures of C1-RasGRP in complex with these ligands and phorbol 13-acetate using a computational docking method. The structural model of C1-RasGRP exhibits a folding pattern that is nearly identical to that of C1b-PKCδ and is comprised of three antiparallel-strand β-sheets capped against a C-terminal α-helix. Two loops A and B comprising residues 8−12 and 21−27 form a binding pocket that has some positive charge character. The ligands phorbol 13-acetate, benzolactam, and ILV are recognized by C1-RasGRP through a number of hydrogen bonds with loops A and B. In the models of C1-RasGRP in complex with phorbol 13-acetate, benzolactam, and ILV, common hydrogen bonds are formed with two residues Thr12 and Leu21, whereas other hydrogen bond interactions are unique for each ligand. Furthermore, our modeling results suggest that the shallower insertion of ligands into the binding pocket of C1-RasGRP compared to C1b-PKCδ may be due to the presence of Phe rather than Leu at position 20 in C1-RasGRP. Taken together, our experimental and modeling studies provide us with a better understanding of the structural basis of the binding of PKC ligands to the novel phorbol ester receptor RasGRP.

Introduction

The Ras guanyl releasing protein (RasGRP) is expressed in the thymus, brain, spleen, and several lymphoid cell lines.[1] It modulates the Ras family of small GTPases that are essential elements in the signal transduction pathways in the cells and plays a crucial role in the regulation of cell growth and cytoskeletal rearrangements.[2] RasGRP functions as an upstream Ras activator through rapid conversion of the inactive GDP-bound Ras to the active GTP-bound form on the inner surface of the plasma membrane.[3] The GTP bound state of Ras is able to bind and activate multiple downstream effectors such as Raf kinase and phosphatidylinositol 3-kinase that then initiate subsequent signaling cascades.[4] The GTPases thus serve as switches for the propagation and divergence of signaling pathways.[5]

One interesting feature of RasGRP is the presence of a C-terminal cysteine-rich domain (also known as the C1 domain),[1,6] which possesses high homology to the C1 domain of protein kinase C (PKC).[7] The deletion of the RasGRP C1 domain (C1-RasGRP) and the reattachment of the PKCδ C1b domain (C1b-PKCδ) or C1-RasGRP to the C1-domain-deleted mutant revealed that the transforming activity of RasGRP is dependent on the presence of the C1 domain.[1]

The C1 domain is a compact zinc-containing motif of ∼50 amino acid residues, which was formerly identified as a conserved region responsible for the activation of PKCs by binding of diacylglycerol (DAG) and phorbol esters.[8] For many years, signaling in response to the second messenger DAG was believed to proceed solely through the activation of one or more PKC isozymes. However, with the identification of RasGRP and other "non-kinase" phorbol ester receptors such as α-/β-chimaerins[9] and *Caenorhabditis elegans* Unc-13,[10] it is now recognized that PKC constitutes only one of five families of receptors for DAG and the phorbol esters. Numerous experiments have shown that the phorbol esters may influence Ras signaling pathways by PKC-dependent pathways.[11,12] A new and direct pathway

* To whom correspondence should be addressed. For A.P.K.: phone, 202-687-0686; fax, 202-687-5065; e-mail, kozikowa@georgetown.edu. For S.W.: phone, 202-687-2028; fax, 202-687-4032; e-mail, wangs@giccs.georgetown.edu.
[†] Georgetown University Medical Center.
[‡] Current address: NeuroLogic Incorporation, 9700 Great Seneca Highway, Rockville, MD 20850.
[§] Shanghai Institute of Organic Chemistry.
[∥] National Cancer Institute.
[⊥] University of Alberta.

10.1021/jm010422z CCC: $22.00
Published on Web 01/22/2002

Chart 1

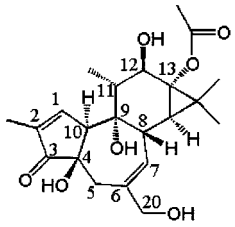

Phorbol 13-acetate

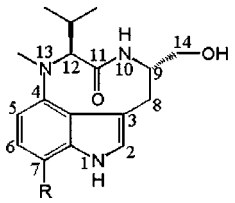

Indolactam V analog

ILV R = H
7-(n-octyl)-ILV R = octyl

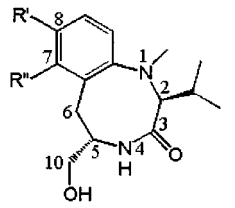

Benzolactam analog

8-(1-decynyl)benzolactam V
(benzolactam)
R′ = 1-decynyl R″ = H

7-methoxy-8-(1-decynyl) benzolactam
(methoxylated benzolactam)
R′ = 1-decynyl R″ = MeO

from DAG to Ras signaling has been revealed by the recruitment of RasGRP to the plasma membrane in response to the binding of DAG and phorbol ester.[1]

RasGRP binds to phorbol 12,13-dibutyrate (PDBu) with nanomolar affinity through its C1 domain.[13] Structure−activity analysis of several phorbol esters revealed that the ligand selectivity of C1-RasGRP is somewhat different from that of C1b-PKC[13] and that the binding of C1-RasGRP to phorbol esters is dependent on the presence of phospholipids.

The binding mode of phorbol 13-acetate to C1b-PKCδ has been determined by X-ray crystallography.[14] NMR spectroscopy, molecular modeling, and site-directed mutagenesis have also been used to investigate the interaction of other PKC ligands with the C1 domains of PKCα, PKCδ, and β_2-chimaerin.[15] Here, we report our experimental and molecular modeling analysis of RasGRP binding to several high-affinity PKC ligands (see Chart 1).

Materials and Methods

Expression and Purification of RasGRP and PKCδ. The C1 domain of rat RasGRP (C1-RasGRP) and the second C1 domain of mouse PKCδ (C1b-PKCδ) were subcloned into a pGEX vector to produce GST fusion proteins in *E. coli*. The proteins were then purified using glutathione Sepharose 4B beads as described elsewhere.[16] Note that the sequence of C1-RasGRP in the present study corresponds to that from SWISS-PROT (O88469), whereas we previously characterized[13] the RasGRP variant rbc7 in which Gly is replaced by Glu in position 35.[1]

Binding Experiments. Binding assays were performed by the poly(ethylene glycol) precipitation method.[17] The binding mixture contained 50 mM Tris-HCl, pH 7.4, 1 mg/mL bovine immunoglobulin G, 0.1 mM $CaCl_2$, 100 μg/mL of sonicated phosphatidylserine, the protein to be assayed, and [^{3}H]PDBu (2 nM) in the absence or presence of different concentrations of the compound being assayed. Incubations were carried out for 5 min at 18 °C for C1-RasGRP or 37 °C for C1b-PKCδ. Nonspecific binding was measured using an excess of nonradioactive PDBu (30 μM). Binding inhibition curves were determined with six to seven concentrations of the inhibitor, with triplicate values at each concentration in each experiment. Mean K_i values were calculated from a minimum of three separate experiments. Indolactam(V) (ILV) and *n*-octyl-ILV were from LC Laboratories (Woburn, MA). 8-(1-Decynyl)benzolactam(V) (benzolactam) and 7-methoxy-8-(1-decynyl)benzolactam(V) (methoxylated benzolactam) were synthesized as described previously.[18]

Sequence Alignment and Homology Modeling. The necessary sequence alignment data were retrieved from two different sources, one of these being a FASTA search of the Protein Data Bank (PDB)[19] while the other made use of the protein family (Pfam) database.[20] From the sequence alignment, a 3D structural model of C1-RasGRP was constructed employing the Homology module implemented in InsightII (Molecular Simulation, Inc., San Diego, CA) and the crystal structure of C1b-PKCδ (PDB 1PTR) as template. Two Zn^{2+} ions extracted from the template protein were merged into the structural model of C1-RasGRP.

The initial model was refined in a stepwise manner by energy minimization with a stand-alone version of the CHARMM program[21] (version c27b2) and the all-atom version 22 force field.[22] First, the model was solvated by a 20 Å sphere of TIP3P water molecules[23] and energetically minimized for 2500 steps, with a fixed backbone, using the adopted-basis Newton−Raphson (ABNR) method to remove the unfavorable contacts. Then, the model was minimized for 2500 steps using harmonic constraints with a force constant of 10.0 kcal mol^{-1} Å^{-2} on the backbone, followed by another 2500 steps of minimization with a force constant of 5.0 kcal mol^{-1} Å^{-2} on the α-carbons. Finally, the whole model was minimized for 2500 steps or until an energy gradient of less than 0.05 kcal mol^{-1} Å^{-1} was achieved. The final model of C1-RasGRP was examined using the 3D profile approach[24] and checked by the program PROCHECK[25] to verify its folding and stereochemical quality.

Docking and Complex Modeling. The structure of phorbol 13-acetate was directly retrieved from the crystal structure of its complex with C1b-PKCδ (PDB 1PTR).[14] The other molecules, including ILV and benzolactam, were modeled using the InsightII/Discover molecular modeling package.

Computational docking was performed using an automated docking method Autodock.[26] First, the crystal structure of C1b-PKCδ in complex with phorbol 13-acetate taken from PDB[14] was used to validate the docking quality achieved by the Autodock program. Next, the three ligands phorbol 13-acetate, ILV and benzolactam were docked sequentially into the binding pocket of the model of C1-RasGRP formed by two loops comprising residues 8−12 and 21−27 (using consensus numbering for the C1 domains). In each case, 50 genetic algorithm dockings and energy evaluations were performed, followed by the cluster analysis based on a root-mean-square deviation tolerance of 0.5 Å. The lowest energy docked structure was selected as the starting complex model. The complex model soaked by a 20 Å sphere of water molecules was optimized by energy minimization for 10 000 steps or until an energy gradient of less than 0.05 kcal mol^{-1} Å^{-1} was reached.

MD Simulation and Analysis. The minimized complex models, together with a 20 Å sphere of water molecules, were used as the starting structures in the molecular dynamics (MD) simulations. The MD simulations were performed with a 10 ps heating period and a 40 ps equilibration, followed by

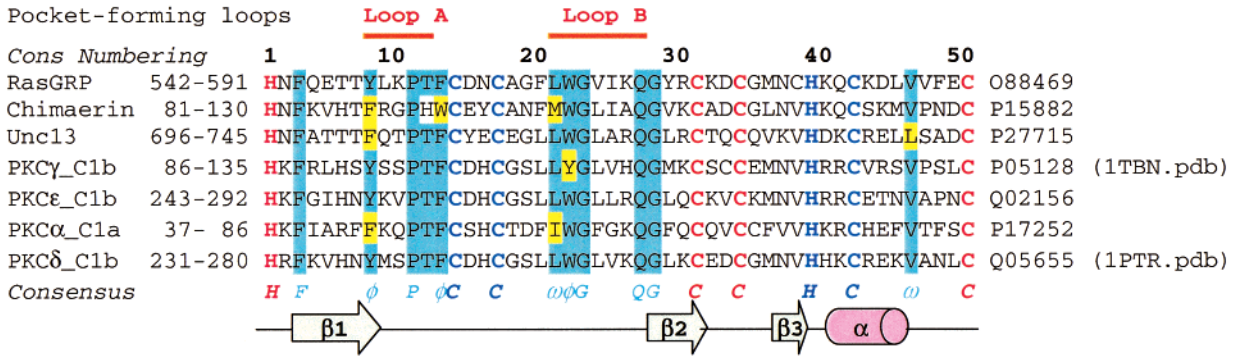

Figure 1. Sequence alignment of C1 domains. The SWISS-PROT accession numbers and PDB entries are indicated at the end of sequences. Consensus sequence numbering and amino acids are shown above and below the sequence alignment, respectively. ϕ and ω represent aromatic and aliphatic hydrophobic amino acids, respectively. Two clusters of the residues coordinating two Zn^{2+} ions are red and blue, respectively. The two binding pocket-forming loops A and B are indicated for the template protein by two orange bars at the top. Secondary structure elements of the template protein, C1b-PKCδ, are shown at the bottom. The green arrows and pink cylinder represent β-strands and α-helix, respectively.

a 100 ps constant temperature simulation at 300 K with a step size of 0.001 ps. The nonbonded energies and forces were smoothly shifted to zero at 12.0 Å,[27] and a dielectric constant was set to 1 for electrostatic interactions. The nonbonded list, including neighboring atoms within a 14.0 Å distance, was updated every 0.5 ps. All bonds to hydrogens were constrained with the SHAKE algorithm.[28] Trajectories were recorded every 0.5 ps of simulation for analysis. All MD simulations were performed on a Beowulf cluster with 450 MHz Pentium III CPU processors.

To examine the conformational changes upon ligand binding, the root-mean-square deviations (rmsd's) of the binding pocket were calculated from the trajectory at 0.5 ps intervals, with the initial structure as the reference.

Since hydrogen bonds are crucial for the interactions between PKC ligands and C1 domains,[14,15] we examined the hydrogen bonding interactions based on the trajectories of the MD simulations. For the analysis of hydrogen bond interactions, a hydrogen bond (D−H···A) was defined by a distance between the donor and acceptor atoms of less than 3.0 Å and an angle θ_{D-H-A} of more than 120°. The percent occupancy and lifetime as well as the energy of the hydrogen bonds were calculated to evaluate the stability and the strength of the hydrogen bonds.

Results and Discussion

Experimental Determination of Ligand Binding Affinities. The compounds ILV, *n*-octyl-ILV, benzolactam, and methoxylated benzolactam were tested for their ability to displace [^{3}H]PDBu binding from C1-RasGRP and C1b-PKCδ. The binding affinity data are presented in Table 1 along with the binding affinities to C1b-PKCδ as determined previously.[15] As can be seen in Table 1, the compounds fall into two categories based on their binding affinities for C1-RasGRP. The first group, including ILV and *n*-octyl-ILV, shows binding affinities around 1 nM for C1-RasGRP, with ILV being 3 times weaker than *n*-octyl-ILV. The second group comprises the two benzolactams. These two ligands are slightly less potent than ILV and *n*-octyl-ILV but still show binding affinities around 10 nM. The methoxylated benzolactam is about 2-fold less potent than benzolactam. Relative to C1b-PKCδ, C1-RasGRP binds the ligands with affinities ranging from 3-fold stronger to 8-fold weaker.

Homology Modeling. (a) Sequence Alignment. The sequence alignments either obtained from the PDB FASTA search or taken directly from the Pfam database are identical and show 50% sequence identity and 70% similarity to the template protein (PDB 1PTR).[14] Since a sequence identity above 50% generally guarantees that the modeled protein structure is correct at a level comparable to that of an X-ray crystal structure,[29] the sequence alignment (Figure 1) obtained from these two sources was used to model C1-RasGRP without any further modification.

Table 1. Binding Affinities to C1-RasGRP and C1b-PKCδ[a]

compd	K_i, RasGRP (nM)	K_i, PKCδ (nM)
ILV	2.54 ± 0.16	2.01 ± 0.17[b]
n-octyl-ILV	0.85 ± 0.01	0.10 ± 0.01[d]
benzolactam	6.15 ± 0.41	10.7 ± 0.8[c]
methoxylated benzolactam	13.92 ± 0.78	35.1 ± 2.3

[a] K_i values were determined from binding inhibition curves using [^{3}H]PDBu as the labeled ligand. Values represent the mean ± SEM of three or more experiments per compound. [b] Reference 15c. [c] Reference 15d. [d] Reference 10b.

The sequence alignment shows that the Zn^{2+} coordinating residues are conserved in all aligned sequences. In fact, these residues are completely conserved in all members of the C1 domain family.[20] On the basis of this conservation, two Zn^{2+} ions taken from the template protein were directly merged into the structural model of C1-RasGRP. In addition, the sequence alignment also contains 11 conserved amino acid residues, including four aromatic and two aliphatic hydrophobic residues, as well as two glycines, two glutamines, and one proline. It is noted that the two most conserved regions are distributed between the β1 and β2 strands, which correspond to loops A and B of the template protein that form the binding pocket (Figure 1).

(b) Structural Model of C1-RasGRP. The 3D profiles verification[24] method shows that the 3D/1D scores of our model are always positive and are similar to those of the template protein (Figure 2), which are within the range of scores for X-ray structure determinations. Additionally, PROCHECK[25] confirms that our model of C1-RasGRP not only has the correct folding but also possesses reasonable geometric structural parameters. Thus, it is expected that the structural model of C1-RasGRP is of sufficiently high quality to be used to investigate the ligand−protein interactions.

Identical to that of C1b-PKCδ, the modeled 3D structure of C1-RasGRP is made up of an antiparallel β-sheet, comprising three strands β1, β2, and β3, and

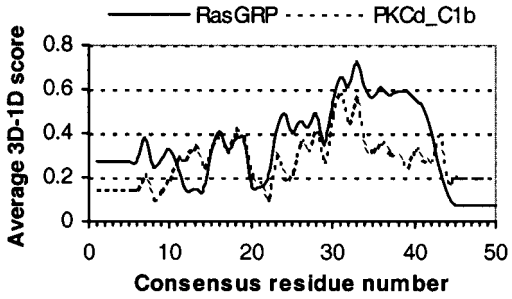

Figure 2. Plots obtained by the Verify3D program with a window of 10 residues using the coordinates of C1-RasGRP and the template protein (C1b-PKCδ, PDB 1PTR), respectively.

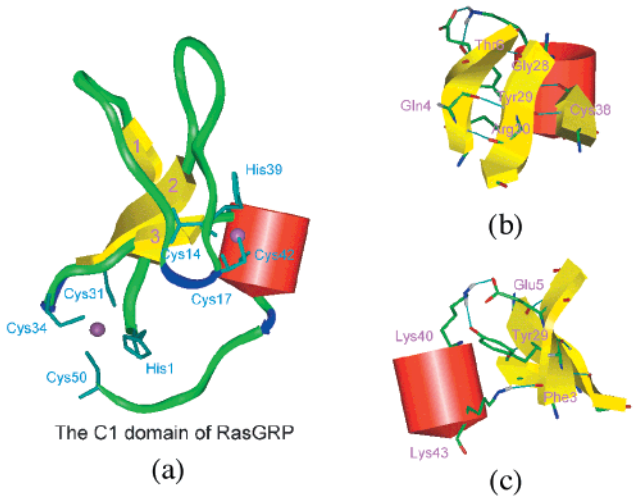

Figure 3. Structural model of C1-RasGRP. (a) Schematic drawing of the model. The β-strands, α-helix, turn, and coils are shown as the yellow arrow, red cylinder, blue ribbon, and green ribbon, respectively. Two Zn^{2+} ions and their coordinating residues are displayed as ball-and-stick models, respectively. (b) View is rotated 270° along the *Y* axis of panel a. Five hydrogen bonds are formed within the β-sheet. (c) View is rotated 180° along the *Y* axis of panel a and then −25° along the *X* axis. Three hydrogen bonds are formed between the α-helix and the β-sheet.

of a C-terminal α-helix proximate to the β-sheet. The domain scaffold is maintained by these three β-strands packed against the α-helix together with two independent zinc ions coordinated by two pairs of 3Cys−1His Zn^{2+} coordinating clusters (Figure 3).

Docking Studies. The docking test showed that the Autodock program could reproduce the binding of phorbol 13-acetate to C1b-PKCδ because the rms value is only 0.77 Å when the lowest energy docked structure was superimposed with the crystal structure. The hydrogen bond network predicted by the Autodock program is virtually identical to that found in the crystal structure. This docking test provides validation for using this program to perform docking studies of ligands to C1-RasGRP.

ILV exists in solution in two different conformations.[30] Both experimental evidence and molecular modeling studies have revealed that ILV adopts the cis−twist conformation when it binds to C1b-PKCδ.[15,30,31] Similarly, the benzolactam, whose eight-membered ring forces the amide bond to be in the cis configuration, adopts a cis−twist conformation in order to bind to C1b-PKCδ.[15] Therefore, the cis−twist conformation was used for docking of these ligands to C1-RasGRP.

In the current modeling studies, we focused on the interaction between the ligands and C1-RasGRP and did not take into account the lipid interactions. For this reason, the hydrophobic side chains of both 7-*n*-octyl-ILV and benzolactam were truncated to four carbon atoms to expedite the docking studies.

Analysis of the Complex Models. (a) Ligand-Binding Pocket. The two loops A and B comprising residues 8−12 and 21−27 make up the ligand-binding pocket (Figures 1, 4, and 6). This binding pocket has some positive charge character. In the complex models, the three ligands phorbol 13-acetate, ILV, and benzolactam interact with loops A and B of RasGRP through complementary hydrogen bonds. All three ligands form hydrogen bonds with residues Thr12 and Leu21.

(b) Conformational Changes of the Binding Pocket upon Ligand Binding. To investigate the effect of ligand binding on the binding pocket conformation, the rmsd's have been calculated from the trajectories of a 100 ps MD production run for loops A and B (Table 2). Table 2 shows that upon ligand binding the rmsd values of loops A and B are reduced 3 and 4 times, respectively. This suggests that the binding pocket formed between loops A and B becomes less flexible upon ligand binding.

The distances between the α-carbons were also calculated for five pairs of residues on loops A and B (Table 3). Table 3 shows that the middle portion of the binding pocket opens up by ∼0.5 Å upon ligand binding (Cα,Lys10−Cα,Val24 and Cα,Pro11−Cα,Gly23). This induced conformational change in the binding pocket upon ligand binding is consistent with the reported X-ray crystallography study, which showed that the binding of phorbol 13-acetate leads to an opening of 0.4 Å between the main chains of Pro11 and Gly23 in C1b-PKCδ.[14]

(c) Hydrogen Bonds Maintaining the Binding Pocket Conformation. We found that the conformation of the binding pocket is maintained by the presence of six hydrogen bonds formed between loops A and B (Figure 5 and Table 4). For uncomplexed C1-RasGRP, only two of these hydrogen bonds between loops A and B exhibit more than 90% occupancy over a 30 ps average lifetime; one is formed by the amide H atom of Leu21 and the carbonyl O atom of Thr12, and the other occurs between the side chain's carbonyl O atom of Gln27 and the amide H atom of Tyr8. Upon ligand binding, in addition to these two stable hydrogen bonds, another stable hydrogen bond appears between the side chain's amide H atom of Gln27 and the carbonyl O atom of Tyr8 (occupancy, 100%; average lifetime, 50 ps; energy, −2.93 ± 0.26 kcal/mol). These more stable hydrogen bonds are located at the two ends of the binding pocket. In contrast, the hydrogen bonds existing at the middle of the binding pocket become less stable, or disappear, upon ligand binding (occupancy, less than 10%; average lifetime, less than 1 ps), thus resulting in the ∼0.5 Å opening in the middle portion of the binding pocket upon ligand binding.

Hydrogen Bonding Interactions between Ligands and C1-RasGRP. All hydrogen bonding interactions between C1-RasGRP and the ligands were

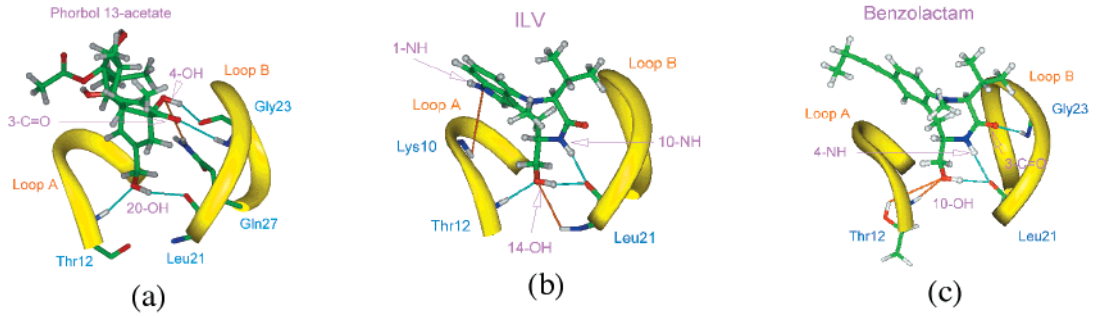

Figure 4. Hydrogen bond interactions between the ligands and C1-RasGRP. (a) The phorbol 13-acetate−C1-RasGRP complex. View is rotated 30° along the *X* axis of Figure 3a. (b) The ILV−C1-RasGRP complex. View is rotated −10° along the *Y* axis of panel a. (c) The benzolactam−C1-RasGRP complex. View is rotated −15° along the *Y* axis of panel a. During the MD simulations, the O atom of benzolactam's 4-OH group forms a hydrogen bond, alternatively, with the amide H atom (light blue) and the side chain's hydroxyl O atom (orange) of Thr12.

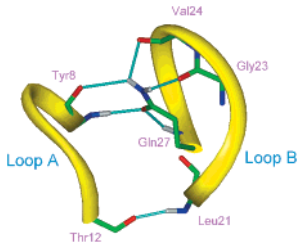

Figure 5. Hydrogen bonds formed between two binding pocket-forming loops A and B. View is rotated −15° along the *X* axis of Figure 3a.

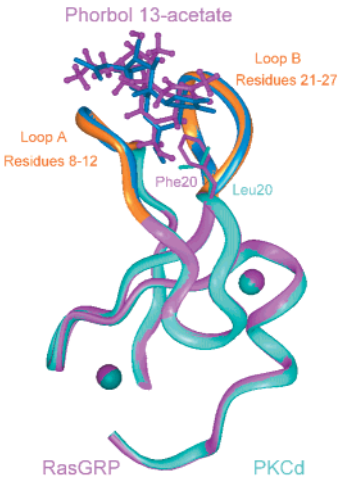

Figure 6. Structural model of C1-RasGRP in complex with phorbol 13-acetate superimposed with C1b-PKC*δ* in complex with phorbol 13-acetate (PDB 1PTR). The view is the same as the view in Figure 3a. The binding pocket-forming loops A and B are pink and blue, respectively, for the C1-RasGRP and C1b-PKC*δ*. The ligand's location within C1-RasGRP is different from that within C1b-PKC*δ*.

analyzed on the basis of the MD trajectories of the complex models (Figure 4, Table 5).

(a) ILV−RasGRP Complex. Three residues in C1-RasGRP form five hydrogen bonds with ILV. Leu21 forms three hydrogen bonds with ILV: the first between its amide group and the hydroxyl group at position 14 in ILV, the second between its carbonyl group and the amide group in ILV, and the third hydrogen bond between its carbonyl group and the hydroxyl group at position 14. Lys10 forms one hydrogen bond through its backbone with the amino group at position 1 in ILV. Thr12 also forms one hydrogen bond through its backbone amide with the hydroxyl group at position 14 in ILV. On the basis of the occupancy, average lifetime, and hydrogen bond energy estimated for each of these five hydrogen bonds (Table 5), two hydrogen bonds are very stable and have the strongest hydrogen bond energies ($O_{14-OH}\cdots HN_{Thr12}$ and $H_{14-OH}\cdots O_{Leu21}$).

Table 2. Root-Mean-Square Deviation (Å) of Two Binding Pocket-Forming Loops

	loop A (residues 8−12)		loop B (residues 21−27)	
	RasGRP	complex[a]	RasGRP	complex[a]
amino acids	0.5577	0.2267	0.8874	0.2216
backbone	0.3191	0.1356	0.5998	0.1443
side chain	0.5848	0.2003	0.9010	0.2116

[a] In complex with phorbol 13-acetate.

Table 3. Distance (Å) between Two Binding Pocket-Forming Loops of C1-RasGRP

	RasGRP	complex[a]
Cα,Tyr8−Cα,Lys26	7.07 ± 0.16	6.97 ± 0.11
Cα,Leu9−Cα,Ile25	9.16 ± 0.16	9.02 ± 0.11
Cα,Lys10−Cα,Val24	9.52 ± 0.14	10.12 ± 0.13
Cα,Pro11−Cα,Gly23	10.26 ± 0.12	10.73 ± 0.12
Cα,Thr12−Cα,Trp22	9.11 ± 0.10	9.04 ± 0.13

[a] In complex with phorbol 13-acetate.

(b) Benzolactam−RasGRP Complex. Thr12, Leu21, and Gly23 in C1-RasGRP form hydrogen bonds with the benzolactam (Figure 4, Table 5). Thr12 forms two hydrogen bonds through its backbone amide and its side chain hydroxyl groups with the hydroxyl O atom at position 10 in benzolactam. Leu21 forms two hydrogen bonds through its backbone carbonyl group with the hydroxyl H atom at position 10 and the amide H atom at position 4 in the ligand. Gly23 forms one hydrogen bond through its amide group with the carbonyl group at position 3. The two hydrogen bonds formed between Leu21 and the ligand ($H_{10-OH}\cdots O_{Leu21}$ and $H_{4-NH}\cdots O_{Leu21}$) were found to be the most stable and have the highest hydrogen bond energies (Table 5).

Comparison of Ligand−Hydrogen Bond Interactions to C1-RasGRP and C1b-PKC*δ*. To gain further insight into ligands binding to C1-RasGRP, we compared the predicted binding model of phorbol 13-acetate in complex with C1-RasGRP and the X-ray structure of the same ligand with C1b-PKC*δ*. It was found that these two protein structures are virtually superimposed with an rmsd value of 0.16 Å for the backbone α-carbon atoms. The major difference is residue 20. C1b-PKC*δ* has a Leu residue at this position,

Table 4. Hydrogen Bonds Maintaining the Binding Pocket Conformation

hydrogen bond	occupancy (%)		average lifetime (ps)		HB parameter and energy			
	a	*b*	*a*	*b*	r_{DA} (Å)	θ_{D-H-A} (deg)	θ_{H-A-AA} (deg)	E_{HB} (kcal/mol)
				RasGRP				
$HN_{Leu21}\cdots O_{Thr12}$	100	100	100.00	100.00	2.84 ± 0.07	157.7 ± 10.2	146.9 ± 9.4	−3.45 ± 0.07
$HE22_{Gln27}\cdots O_{Gly23}$	23	23	2.67	2.30	2.83 ± 0.14	108.3 ± 13.9	129.6 ± 7.4	−3.33 ± 0.27
$OE1_{Gln27}\cdots HN_{Gln27}$	72	70	2.50	3.50	3.00 ± 0.14	124.8 ± 8.1	120.5 ± 5.3	−3.39 ± 0.14
$OE1_{Gln27}\cdots HN_{Tyr8}$	99.5	100	49.75	100.00	2.98 ± 0.15	149.0 ± 11.3	128.9 ± 9.2	−3.40 ± 0.15
$HE21_{Gln27}\cdots O_{Val24}$	14	17	1.17	1.42	3.89 ± 0.24	40.5 ± 11.6	77.4 ± 6.0	−2.03 ± 0.42
$HE21_{Gln27}\cdots O_{Tyr8}$	35	36	1.50	1.56	3.85 ± 0.21	39.0 ± 7.6	107.7 ± 5.8	−2.10 ± 0.36
				Complex[c]				
$HN_{Leu21}\cdots O_{Thr12}$	98.5	98	32.83	32.67	2.98 ± 0.10	152.2 ± 14.4	150.2 ± 10.6	−3.44 ± 0.08
$HE22_{Gln27}\cdots O_{Gly23}$	11	9	1.00	1.12	3.51 ± 0.18	111.4 ± 7.8	117.4 ± 5.3	−2.68 ± 0.31
$OE1_{Gln27}\cdots HN_{Gln27}$	85	85	4.39	6.07	2.82 ± 0.11	133.0 ± 12.7	111.7 ± 5.5	−3.37 ± 0.18
$OE1_{Gln27}\cdots HN_{Tyr8}$	100	100	100.00	100.00	3.30 ± 0.16	154.3 ± 8.4	92.8 ± 6.1	−3.02 ± 0.25
$HE21_{Gln27}\cdots O_{Val24}$	0.0	2	0.00	1.00	3.39 ± 0.24	45.2 ± 5.97	82.8 ± 4.5	−2.88 ± 0.32
$HE21_{Gln27}\cdots O_{Tyr8}$	99.5	100	49.75	100.00	3.35 ± 0.16	49.5 ± 6.3	124.7 ± 6.6	−2.93 ± 0.26

[a] Time cutoff 0.5 ps, resolution 0.5 ps. [b] Time cutoff 0.5 ps, resolution 1.0 ps. [c] In complex with phorbol 13-acetate.

Table 5. Hydrogen Bond Interactions between C1-RasGRP and the Ligands

hydrogen bond $atom_{ligand}\cdots atom_{residue}$	occupancy (%)		average lifetime (ps)		hydrogen bond parameter and energy			
	a	*b*	*a*	*b*	r_{DA} (Å)	θ_{D-H-A} (deg)	θ_{H-A-AA} (deg)	E_{HB} (kcal/mol)
				ILV				
$H_{10-NH}\cdots O_{Leu21}$	9.50	11.00	1.00	1.00	3.88 ± 0.26	123.7 ± 9.3	139.1 ± 7.6	−2.06 ± 0.26
$N_{1-NH}\cdots HN_{Lys10}$	50.00	52.00	1.73	2.60	3.04 ± 0.12	119.1 ± 10.6	94.4 ± 5.5	−2.94 ± 0.08
$O_{14-OH}\cdots HN_{Thr12}$	99.00	98.00	49.25	49.00	2.97 ± 0.13	149.1 ± 12.5	116.2 ± 11.0	−3.42 ± 0.11
$O_{14-OH}\cdots HN_{Leu21}$	28.00	28.00	1.35	1.56	3.76 ± 0.14	127.6 ± 9.6	147.9 ± 5.7	−2.25 ± 0.22
$H_{14-OH}\cdots O_{Leu21}$	98.00	98.00	19.60	32.67	2.84 ± 0.12	141.4 ± 9.9	121.0 ± 6.9	−4.13 ± 0.14
							total	−14.8
				Benzolactam				
$O_{3-C=O}\cdots HN_{Gly23}$	52.00	55.00	2.25	2.62	2.78 ± 0.11	120.8 ± 11.7	123.9 ± 8.3	−3.32 ± 0.20
$O_{10-OH}\cdots HN_{Thr12}$	59.50	61.00	1.88	2.54	2.77 ± 0.10	124.2 ± 13.3	145.6 ± 6.9	−3.32 ± 0.21
$O_{10-OH}\cdots HG1_{Thr12}$	67.50	71.00	2.40	4.18	3.66 ± 0.13	132.8 ± 6.7	88.1 ± 4.7	−2.54 ± 0.24
$H_{10-OH}\cdots O_{Leu21}$	100.00	100.00	100.00	100.00	2.84 ± 0.12	141.4 ± 9.9	121.0 ± 6.9	−4.13 ± 0.14
$H_{4-NH}\cdots O_{Leu21}$	99.50	100.00	49.75	100.00	2.96 ± 0.11	154.6 ± 11.3	150.9 ± 9.4	−3.44 ± 0.08
							total	−16.75

[a] Time cutoff 0.5 ps, resolution 0.5 ps. [b] Time cutoff 0.5 ps, resolution 1.0 ps.

while C1-RasGRP has a Phe residue. For the ligand, its position is shifted up by 0.7 Å from the bottom of the binding pocket in the complex with C1-RasGRP versus PKCδ because of the residue difference at position 20 (Figure 6).

For phorbol 13-acetate,[14] four common, strong hydrogen bonds are formed with C1b-PKCδ and C1-RasGRP (in light blue in Figure 4a). One difference in the hydrogen bonding network is that there is a weak hydrogen bond formed between the hydroxyl group at position 20 and the carbonyl group of Thr12 in the X-ray structure, while this hydrogen bond is replaced by another weak hydrogen bond between the hydroxyl group at position 4 in the ligand and the side chain's amide of Gln27 in the predicted RasGRP−phorbol 13 acetate complex (in orange in Figure 4a).

For ILV,[15] three common hydrogen bonds are found with C1-RasGRP and C1b-PKCδ (light blue in Figure 4b). Interestingly, the hydrogen bond between the carbonyl group at position 11 and the amide group of Gly23 in the ILV/PKCδ complex was replaced by two hydrogen bonds in the predicted ILV−RasGRP complex; one occurs between the hydroxyl group at position 14 of the ligand and the amide group of Leu21, and the other is formed by the amino group at position 1 and the amide group of Lys10 (in orange in Figure 4b).

For benzolactam, four common hydrogen bonds are found with both C1b-PKCδ and C1-RasGRP residues Thr12, Leu21, and Gly23.[15] However, a minor difference is observed in the hydrogen bonding interactions with Thr12. In the C1b-PKCδ complex, the hydroxyl group at position 10 of the ligand forms only one hydrogen bond with the backbone amide of Thr12. In the RasGRP complex this hydroxyl group forms two alternating hydrogen bonds during the MD simulations, one with the amide H atom of Thr12 and the other with side chain's hydroxyl H atom of Thr12 (in orange in Figure 4c).

The differences in the ligand−hydrogen bond interactions with C1b-PKCδ and C1-RasGRP may stem from differences in the residue at position 20, since this specific residue is located at the edge of the binding pocket while all the other dissimilar residues at positions 8, 9, 24, 25, and 26 are directed outside the binding pocket. Since Phe is slightly larger than Leu in their side chains, Phe20 in C1-RasGRP may cause the ligand to shift upward slightly in order to avoid steric contacts, thus leading to a weakening of hydrogen bonding interactions at the Thr12/Leu21 end of the binding pocket. It should be noted, however, that the mutation of C1b-PKCδ at position 20 from Leu to Phe had little effect on the binding affinity of PDBu.[15]

Summary

Binding assays were performed to assess the affinities of several PKC activators for C1-RasGRP. The two benzolactam analogues studied were found to bind to C1-RasGRP in the nanomolar range. ILV and its *n*-octyl

derivative show the best affinities. All four ligands show generally similar affinities for C1-RasGRP and for C1b-PKCδ, although some selectivity is apparent.

Our molecular modeling studies reveal that the interactions of C1-RasGRP with phorbol 13-acetate, benzolactam, and ILV share a common structural feature; i.e., their hydroxymethyl-bearing rings are all inserted in a complementary fashion into the binding pocket formed by loops A and B comprising residues 8−12 and 21−27. In particular, the hydroxymethyl group of phorbol 13-acetate, benzolactam, and ILV plays a pivotal role in C1-RasGRP binding. This group contacts the bottom of the binding pocket, forming hydrogen bonds with Thr12 and Leu21. Some differences do, however, exist among the interactions of these ligands with C1-RasGRP.

The molecular modeling studies also show that the similar 3D structures of C1-RasGRP and C1b-PKCδ result in their common mode of interaction with various ligands, but the difference at residue 20 between these two domains is likely responsible for the lesser depth of penetration of ligands into the binding pocket of C1-RasGRP in comparison to C1b-PKCδ.

Taken together, our ligand binding experiments and molecular modeling studies further our understanding of the structural basis of the binding of PKC activators to the C1 domain of RasGRP. The studies provide a basis for exploring how other types of PKC ligands bind to C1-RasGRP, and such information may be useful for the design of RasGRP-selective ligands. The recent demonstration that RasGRP plays an early and obligatory role in T cell activation highlights the potential utility of such ligands.[32]

Acknowledgment. This work was supported by NIH Grant CA79601 and the Department of Defense Grant DMAD 17-93-V-3018.

References

(1) (a) Ebinu, J. O.; Bottorff, D. A.; Chan, E. Y.; Stang, S. L.; Dunn, R. J.; Stone, J. C. RasGRP, a Ras guanyl nucleotide-releasing protein with calcium- and diacylglycerol-binding motifs. *Science* **1998**, *280*, 1082−1086. (b) Tognon, C. E.; Kirk, H. E.; Passmore, L. A.; Whitehead, I. P.; Der, C. J.; Kay, R. J. Regulation of RasGRP via a phorbol ester-responsive C1 domain. *Mol. Cell Biol.* **1998**, *18*, 6995−7008.

(2) Macara, I. G.; Lounsbury, K. M.; Richards, S. A.; McKiernan, C.; Bar-Sagi, D. The Ras superfamily of GTPases. *FASEB J.* **1996**, *10*, 625−630.

(3) Downward, J. Control of Ras activation. *Cancer Surv.* **1996**, *27*, 87−100.

(4) (a) Morrison, D. K.; Cutler, R. E. The complexity of Raf-1 regulation. *Curr. Opin. Cell Biol.* **1997**, *9*, 174−179. (b) Robinson, M. J.; Cobb, M. H. Mitogen-activated protein kinase pathways. *Curr. Opin. Cell Biol.* **1997**, *9*, 180−186. (c) Treisman, R. Regulation of transcription by MAP kinase cascades. *Curr. Opin. Cell Biol.* **1996**, *8*, 205−215. (d) Rodriguez-Viciana, P.; Warne, P. H.; Khwaja, A.; Marte, B. M.; Pappin, D.; Das, P.; Waterfield, M. D.; Ridley, A.; Downward, J. Role of phosphatidylinositol 3-OH kinase in cell transformation and control of the actin cytoskeleton by Ras. *Cell* **1997**, *89*, 457−467. (e) Feig, L. A.; Urano, T.; Cantor, S. Evidence for a Ras/Ral signaling cascade. *Trends Biochem. Sci.* **1996**, *21*, 438−441.

(5) (a) Bokoch, G. M.; Der, C. J. Emerging concepts in the Ras superfamily of GTP-binding proteins. *FASEB J.* **1993**, *7*, 750−759. (b) Graham, S. M.; Vojtek, A. B.; Huff, S. Y.; Cox, A. D.; Clark, G. J.; Cooper, J. A.; Der, C. J. TC21 causes transformation by Raf-independent signaling pathways. *Mol. Cell. Biol.* **1996**, *16*, 6132−6140.

(6) Ron, D.; Kazanietz, M. G. New insights into the regulation of protein kinase C and novel phorbol ester receptors. *FASEB J.* **1999**, *13*, 1658−1676.

(7) Hurley, J. H.; Newton, A. C.; Parker, P. J.; Blumberg, P. M.; Nishizuka, Y. Taxonomy and function of C1 protein kinase C homology domains. *Protein Sci.* **1997**, *6*, 477−480.

(8) (a) Nishizuka, Y. Intracellular signaling by hydrolysis of phospholipids and activation of protein kinase C. *Science* **1992**, *258*, 607−614. (b) Newton, A. C. Regulation of protein kinase C. *Curr. Opin. Cell. Biol.* **1997**, *9*, 161−167.

(9) (a) Hall, C.; Monfries, C.; Smith, P. Lim, H. H.; Kozma, R.; Ahmed, S.; Vanniasingham, V.; Leung, T.; Lim, L. Novel human brain cDNA encoding a 34,000 Mr protein n-chimaerin, related to both the regulatory domain of protein kinase C and BCR, the product of the breakpoint cluster region gene. *J. Mol. Biol.* **1990**, *211*, 11−16. (b) Hall, C.; Sin, W. C.; Teo, M.; Michael, G. J.; Smith, P.; Dong, J. M.; Lim, H. H.; Manser, E.; Spurr, N. K.; Jones, T. A. Alpha 2-chimerin, an SH2-containing GTPase-activating protein for the ras-related protein p21rac derived by alternate splicing of the human n-chimerin gene, is selectively expressed in brain regions and testes. *Mol. Cell Biol.* **1993**, *13*, 4986−4998. (c) Leung, T.; How, B.-E.; Manser, E.; Lim, L. Germ cell beta-chimaerin, a new GTPase-activating protein for p21rac, is specifically expressed during the acrosomal assembly stage in rat testis. *J. Biol. Chem.* **1993**, *268*, 3813−3816. (d) Leung, T.; How, B.-E.; Manser, E.; Lim, L. Cerebellar beta 2-chimaerin, a GTPase-activating protein for p21 ras-related rac is specifically expressed in granule cells and has a unique N-terminal SH2 domain. *J. Biol. Chem.* **1994**, *269*, 12888−12892. (e) Areces, L. B.; Kazanietz, M. G.; Blumberg, P. M. Close similarity of baculovirus-expressed n-chimaerin and protein kinase C alpha as phorbol ester receptors. *J. Biol. Chem.* **1994**, *269*, 19553−19558. (f) Caloca, M. J.; Fernandez, N.; Lewin, N. E.; Ching, D.; Modali, R.; Blumberg, P. M.; Kazanietz, M. G. 2-Chimaerin Is a High Affinity Receptor for the Phorbol Ester Tumor Promoters. *J. Biol. Chem.* **1997**, *272*, 26488−26496.

(10) (a) Maruyama, I. N.; Brenner, S. A phorbol ester/diacylglycerol-binding protein encoded by the unc-13 gene of *Caenorhabditis elegans*. *Proc. Natl. Acad. Sci. U.S.A.* **1991**, *88*, 5729−5733. (b) Kazanietz, M. G.; Lewin, N. E.; Bruns, J. D.; Blumberg, P. M. Characterization of the Cysteine-Rich Region of the Caenorhabditiselegans Protein Unc-13 as a High Affinity Phorbol Ester Receptor. *J. Biol. Chem.* **1995**, *270*, 10777−10783.

(11) (a) Cai, H.; Smola, U.; Wixler, V.; Eisenmann-Tappe, I.; Diaz-Meco, M. T.; Moscat, J.; Rapp, U.; Cooper, G. M. Role of diacylglycerol-regulated protein kinase C isotypes in growth factor activation of the Raf-1 protein kinase. *Mol. Cell Biol.* **1997**, *17*, 732−741. (b) Marquardt, B.; Frith, D.; Stabel, S. Signaling from TPA to MAP kinase requires protein−kinase-C, RAF and MEK-reconstitution of the signaling pathway in vitro. *Oncogene* **1994**, *9*, 3213−3218. (c) Schönwasser, D. C.; Marais, R. M.; Marshall, C. J.; Parker, P. J. Activation of the mitogen-activated protein kinase/extracellular signal-regulated kinase pathway by conventional, novel, and atypical protein kinase C isotypes. *Mol. Cell Biol.* **1998**, *18*, 790−798. (d) El-Shemerly, M. Y.; Besser, D.; Nagasawa, M.; Nagamine, Y. 12-*O*-Tetradecanoylphorbol-13-acetate activates the Ras/extracellular signal-regulated kinase (ERK) signaling pathway upstream of SOS involving serine phosphorylation of Shc in NIH3T3 cells. *J. Biol. Chem.* **1997**, *272*, 30599−30602. (e) Lorenzo, P. S.; Kung, J. W.; Bottorff, D. A.; Garfield, S. H.; Stone, J. C.; Blumberg, P. M. Phorbol esters modulate the Ras exchange factor RasGRP3. *Cancer Res.* **2001**, *61*, 943−949.

(12) Marais, R.; Light, Y.; Maison, C.; Paterson, H.; Olson, M. F.; Marshall, C. J. Requirements of Ras-GTP−Raf complexes for activation of Raf-1 by protein kinase C. *Science* **1998**, *280*, 109−112.

(13) Lorenzo, P. S.; Beheshti, M.; Pettit, G. R.; Stone, J. C.; Blumberg, P. M. The Guanine Nucleotide Exchange Factor RasGRP Is a High-Affinity Target for Diacylglycerol and Phorbol Esters. *Mol. Pharmacol.* **2000**, *57*, 840−846.

(14) Zhang, G.; Kazanietz, M. G.; Blumberg, P. M.; Hurley, J. H. Crystal structure of the cys2 activator-binding domain of protein kinase C in complex with phorbol ester. *Cell* **1995**, *81*, 917−924.

(15) (a) Hommel, U.; Zurini, M. Solution Structure of a Cysteine Rich Domain of Rat Protein Kinase C. *Nature Struct. Biol.* **1994**, *1*, 383−387. (b) Ichikawa, S.; Hatanaka, H.; Takeuchi, Y.; Ohno, S.; Inagaki, F. Solution Structure of Cysteine-Rich Domain of Protein Kinase C. *J. Biochem.* **1995**, *117*, 566−574. (c) Wang, S.; Liu, M.; Lewin, N. E.; Lorenzo, P. S.; Bhattacharrya, D.; Qiao, L.; Kozikowski, A. P.; Blumberg, P. M. Probing the binding of indolactam-V to protein kinase C through site-directed mutagenesis and computational docking simulations. *J. Med. Chem.* **1999**, *42*, 3436−3446. (d) Kozikowski, A. P.; Wang, S.; Ma, D.; Yao, J.; Ahmad, S.; Glazer, R. I.; Bogi, K.; Acs, P.; Modarres, S.; Lewin, N. E.; Blumberg, P. M. Modeling, chemistry, and biology of the benzolactam analogues of indolactam V (ILV). 2. Identification of the binding site of the benzolactams in the CRD2 activator-binding domain of PKCδ and discovery of an ILV analogue of improved isozyme selectivity. *J. Med. Chem.* **1997**, *40*, 1316−1326. (e) Caloca, M. J.; Garcia-Bermejo, M. L.; Blumberg, P. M.; Lewin, N. E.; Kremmer, E.; Mischak, H.; Wang, S.; Nacro, K.; Bienfait, B.; Marquez, V. E.; Kazanietz, M. G. Beta2-chimaerin is a novel target for diacylglycerol: binding properties

and changes in subcellular localization mediated by ligand binding to its C1 domain. *Proc. Natl. Acad. Sci. U.S.A.* **1999**, *96*, 11854−11859. (f) Wang, S.; Kazanietz, M. G.; Blumberg, P. M.; Marquez, V. E.; Milne, G. W. Molecular modeling and site-directed mutagenesis studies of a phorbol ester-binding site in protein kinase C. *J. Med. Chem.* **1996**, *39*, 2541−2553. (g) Wang, Q. J.; Fang, T. W.; Nacro, K.; Marquez, V. E.; Wang, S.; Blumberg, P. M. Role of hydrophobic residues in the C1b domain of protein kinase C delta on ligand and phospholipid interactions. *J. Biol. Chem.* **2001**, *276*, 19580−19587.

(16) Kazanietz, M. G.; Wang, S.; Milne, G. W.; Lewin, N. E.; Liu, H. L.; Blumberg, P. M. Residues in the second cysteine-rich region of protein kinase C delta relevant to phorbol ester binding as revealed by site-directed mutagenesis. *J. Biol. Chem.* **1995**, *270*, 21852−21859.

(17) Sharkey, N. E.; Blumberg, P. M. Highly lipophilic phorbol esters as inhibitors of specific [^{3}H]phorbol 12,13-dibutyrate binding. *Cancer Res.* **1985**, *45*, 19−24.

(18) Ma, D.; Zhang, T.; Wang, G.; Kozikowski, A. P.; Lewin, N. E.; Blumberg, P. M. Synthesis of 7,8-disubstituted benzolactam-V8 and its binding to protein kinase C. *Bioorg. Med. Chem. Lett.* **2001**, *11*, 99−101

(19) Berman, H. M.; Westbrook, J.; Feng, Z.; Gilliland, G.; Bhat, T. N.; Weissig, H.; Shindyalov, I. N.; Bourne, P. E. The Protein Data Bank. *Nucleic Acids Res.* **2000**, *28*, 235−242.

(20) (a) Sonnhammer, E. L.; Eddy, S. R.; Durbin, R. Pfam: a comprehensive database of protein domain families based on seed alignments. *Proteins* **1997**, *28*, 405−420. (b) Bateman, A.; Birney, E.; Durbin, R.; Eddy, S. R.; Howe, K. L.; Sonnhammer, E. L. The Pfam Protein Families Database. *Nucleic Acids Res.* **2000**, *28*, 263−266.

(21) Brooks, B. R.; Bruccoleri, R. E.; Olafson, B. D.; States, D. J.; Swaminathan, S.; Karplus, M. CHARMM: A program for macromolecular energy, minimization, and dynamics calculations. *J. Comput. Chem.* **1983**, *4*, 187−217.

(22) (a) MacKerell, A. D.; Wiorkiewicz-Kuczera, J. J.; Karplus, M. An all-atom empirical energy function for the simulation of nucleic acids. *J. Am. Chem. Soc.* **1995**, *117*, 11946−11975. (b) MacKerell, A. D.; Bashford, J. D.; Bellott, M.; Dunbrack, R. L., Jr.; Evanseck, J. D.; Field, M. J.; Fischer, S.; Gao, J.; Guo, H.; Ha, S.; Joseph-McCarthy, D.; Kuchnir, L.; Kuczera, K.; Lau, F. T. K.; Mattos, C.; Michnick, S.; Ngo, T.; Nguyen, D. T.; Prodhom, B.; Reiher, W. E.; Roux, B.; Schlenkrich, M.; Smith, J. C.; Stote, R.; Straub, J.; Watanabe, M.; Wiorkiewicz-Kuczera, J.; Yin, D.; Karplus, M. All-atom empirical potential for molecular modeling and dynamics studies of proteins. *J. Phys. Chem.* **1998**, *102*, 3586−3616.

(23) Jorgensen, W. L.; Chandrasekhar, J.; Madura, J. D.; Impey, R. W.; Klein, M. L. Comparison of simple potential functions for simulating liquid water. *J. Chem. Phys.* **1983**, *79*, 926−935.

(24) Luthy, R.; Bowie, J. U.; Eisenberg, D. Assessment of protein models with three-dimensional profiles. *Nature* **1992**, *356*, 83−85.

(25) Rodriguez, R.; Chinea, G.; Lopez, N.; Pons, T.; Vriend, G. Homology modeling, model and software evaluation: three related resources. *Bioinformatics* **1998**, *14*, 523−528.

(26) Morris, G. M.; Goodsell, D. S.; Halliday, R. S.; Huey, R.; Hart, W. E.; Belew, R. K.; Olson, A. J. Automated Docking Using a Lamarckian Genetic Algorithm and Empirical Binding Free Energy Function. *J. Comput. Chem.* **1998**, *19*, 1639−1662.

(27) Steinbach, P. J.; Brooks, B. R. New spherical-cutoff methods for long-range forces in macromolecular simulation. *J. Comput. Chem.* **1994**, *15*, 667−683.

(28) Ryckaert, J. P.; Ciccotti, G.; Berendsen, H. J. C. Numerical integration of the Cartesian equations of motion of a system with constraints: MD of *n*-alkanes. *J. Comput. Phys.* **1977**, *23*, 327−341.

(29) (a) Chothia, C.; Lesk, A. M. The relation between the divergence of sequence and structure in proteins. *EMBO J.* **1986**, *5*, 823−826. (b) Sánchez, R.; Sali, A. Advances in comparative protein−structure modeling. *Curr. Opin. Struct. Biol.* **1997**, *7*, 206−214. (c) Tramontano, A. Homology modeling with low sequence identity. *Methods* **1998**, *14*, 293−300.

(30) Endo, Y.; Hasegawa, M.; Itai, A.; Shudo, K.; Tori, M.; Asakawa, Y.; Sakai, S. Tumor promoters in two conformational states in solution. Stereochemistry of (±)-Indolactam-V. *Tetrahedron Lett.* **1985**, *26*, 1069−1072.

(31) Kozikowski, A. P.; Ma, D.; Pang, Y.-P.; Shum, P.; Likic, V.; Mishra, P. K.; Macura, S.; Basu, A.; Lazo, J. S.; Ball, R. G. Synthesis, molecular modeling, 2-D-NMR, and biological evaluation of ILV mimics as potential modulators of protein kinase C. *J. Am. Chem. Soc.* **1993**, *115*, 3957−3965.

(32) (a) Ebinu, J. O.; Stang, S. L.; Teixeira, C.; Bottorff, D. A.; Hooton, J.; Blumberg, P. M.; Barry, M.; Bleakley, R. C.; Ostergaard, H. L.; Stone, J. C. RasGRP links T-cell receptor signaling to Ras. *Blood* **2000**, *95*, 3199−3203. (b) Dower, N. A.; Stang, S. L.; Bottorff, D. A.; Ebinu, J. O.; Dickie, P.; Ostergaard, H. L.; Stone, J. C. RasGRP is essential for mouse thymocyte differentiation and TCR signaling. *Nat. Immunol.* **2000**, *1*, 317−321.

JM010422Z